

MiniBooNE Results and Follow-On Experiments

W. C. LOUIS for the MiniBooNE collaboration
*Physics Division, Los Alamos National Laboratory,
Los Alamos, NM 87545, USA*
E-mail: louis@lanl.gov

ABSTRACT

The MiniBooNE experiment at Fermilab was designed to test the LSND evidence for neutrino oscillations ¹⁾. The updated MiniBooNE oscillation result in neutrino mode ²⁾ with 6.5E20 protons on target (POT) shows no significant excess of events at higher energies (above 475 MeV), although a sizeable excess ($128.8 \pm 20.4 \pm 38.3$ events) is observed at lower energies (below 475 MeV), where the first error is statistical and the second error is systematic. The lack of a significant excess at higher energies allows MiniBooNE to rule out simple $2-\nu$ oscillations as an explanation of the LSND signal. However, the low-energy excess is presently unexplained. Additional antineutrino data and NuMI data may allow the collaboration to determine whether the excess is due, for example, to a neutrino neutral-current radiative interaction ³⁾ or to neutrino oscillations involving sterile neutrinos ^{4,5,6,7,8)} and whether the excess is related to the LSND signal.

1. Introduction

Evidence for neutrino oscillations comes from solar-neutrino ^{9,10,11,12,13)} and reactor-antineutrino experiments ¹⁴⁾, which have observed ν_e disappearance at $\Delta m^2 \sim 8 \times 10^{-5}$ eV², and atmospheric-neutrino ^{15,16,17,18)} and long-baseline accelerator-neutrino experiments ^{19,20)}, which have observed ν_μ disappearance at $\Delta m^2 \sim 3 \times 10^{-3}$ eV². In addition, the LSND experiment ¹⁾ has presented evidence for $\bar{\nu}_\mu \rightarrow \bar{\nu}_e$ oscillations at the $\Delta m^2 \sim 1$ eV² scale. If all three phenomena are caused by neutrino oscillations, these three Δm^2 scales cannot be accommodated in an extension of the Standard Model that allows only three neutrino mass eigenstates. An explanation of all three mass scales with neutrino oscillations requires the addition of more than one sterile neutrinos ^{4,5,6,7,8)} or further extensions of the Standard Model (*e.g.*, ²¹⁾).

The MiniBooNE experiment was designed to test the neutrino oscillation interpretation of the LSND signal in both neutrino and antineutrino modes. MiniBooNE has approximately the same L/E_ν as LSND but with an order of magnitude higher baseline and energy. Due to the higher energy and dissimilar event signature, MiniBooNE systematic errors are completely different from LSND errors. MiniBooNE's updated oscillation results in neutrino mode ²⁾ show no significant excess of events at higher energies; however, a sizeable excess of events is observed at lower energies, as shown in Fig. 1. Although the excess energy shape does not fit two-neutrino oscillations, the number of excess events agrees approximately with the LSND expectation. At

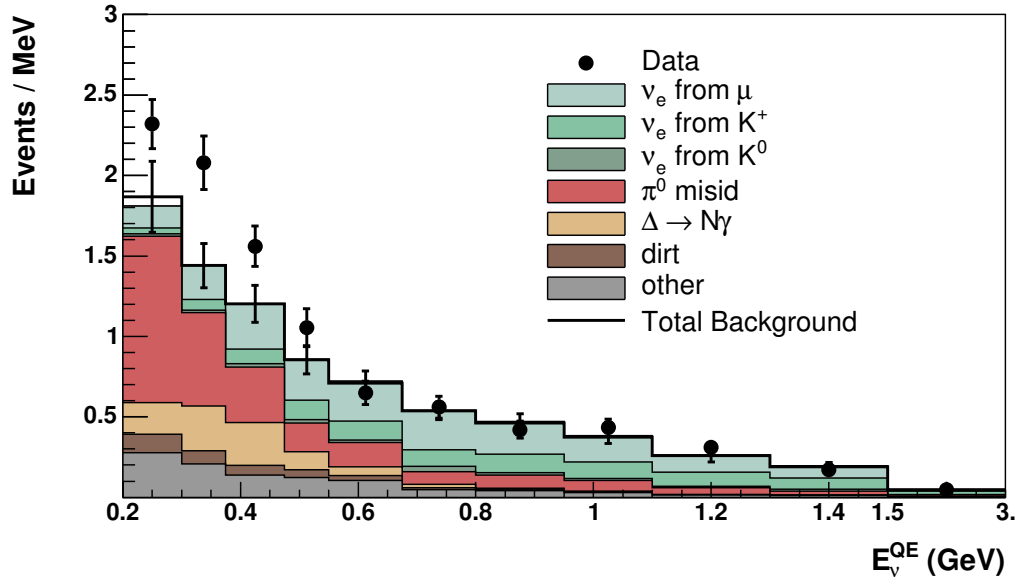


Figure 1: The MiniBooNE reconstructed neutrino energy distribution for candidate ν_e data events (points with error bars) compared to the Monte Carlo simulation (histogram).

present, with $3.4E20$ POT in antineutrino mode, MiniBooNE observes no excess at lower energies.

2. MiniBooNE

2.1. Description of the Experiment

A schematic drawing of the MiniBooNE experiment at FNAL is shown in Fig. 2. The experiment is fed by 8-GeV kinetic energy protons from the Booster that interact in a 71-cm long Be target located at the upstream end of a magnetic focusing horn. The horn pulses with a current of 174 kA and, depending on the polarity, either focuses π^+ and K^+ and defocuses π^- and K^- to form a neutrino beam or focuses π^- and K^- and defocuses π^+ and K^+ to form a less pure antineutrino beam. The produced pions and kaons then decay in a 50-m long pipe, and the resulting neutrinos and antineutrinos²²⁾ can then interact in the MiniBooNE detector, which is located 541 m downstream of the Be target. For the MiniBooNE results presented here, a total of 6.5×10^{20} POT were collected in neutrino mode and 3.4×10^{20} POT were collected in antineutrino mode.

The MiniBooNE detector²³⁾ consists of a 12.2-m diameter spherical tank filled with approximately 800 tons of mineral oil (CH_2). A schematic drawing of the MiniBooNE detector is shown in Fig. 3. There are a total of 1280 8-inch detector phototubes (covering 10% of the surface area) and 240 veto phototubes. The fiducial

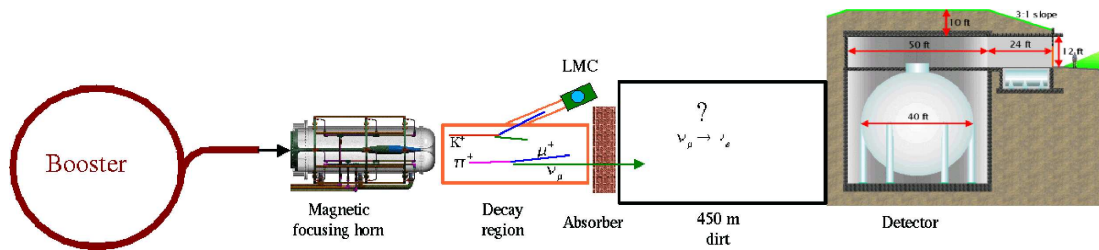


Figure 2: A schematic drawing of the MiniBooNE experiment.

MiniBooNE Detector

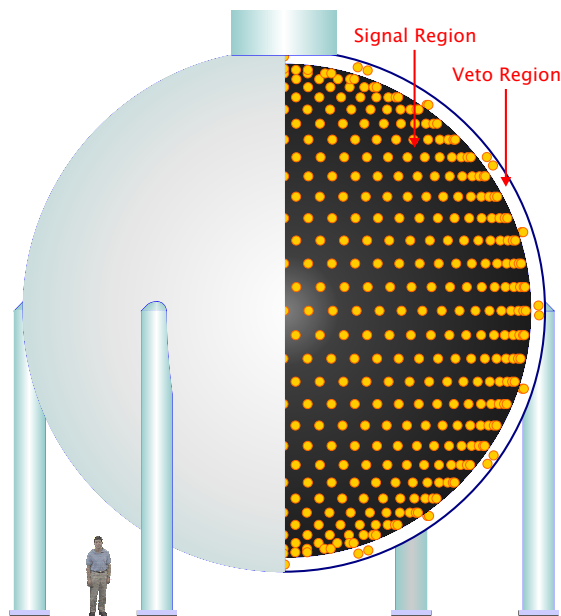


Figure 3: A schematic drawing of the MiniBooNE detector.

volume has a 5-m radius and corresponds to approximately 450 tons. Only $\sim 2\%$ of the phototube channels failed over the course of the run.

2.2. MiniBooNE Cross Section Results

MiniBooNE has published two cross section results. First, MiniBooNE has made a precision measurement of ν_μ charged-current quasi-elastic (CCQE) scattering events²⁴. Fig. 4 shows the ν_μ CCQE Q^2 distribution for data (points with error bars) compared to a MC simulation (histograms). A strong disagreement between the data and the original simulation (dashed histogram) was first observed. However, by increasing the axial mass, M_A , to 1.23 ± 0.20 GeV and by introducing a new variable, $\kappa = 1.019 \pm 0.011$, where κ is the increase in the incident proton threshold, the agreement between data and the simulation (solid histogram) is greatly improved. It

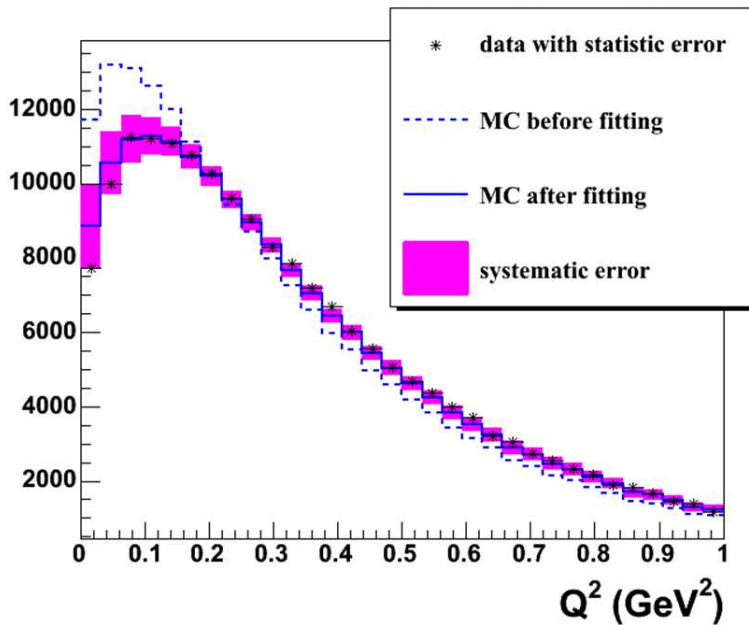


Figure 4: The ν_μ CCQE Q^2 distribution for data (points with error bars) compared to the MC simulation (histograms).

is impressive that such good agreement is obtained by adjusting these two variables.

MiniBooNE has also collected the world's largest sample of neutral-current π^0 events²⁵⁾, as shown in Fig. 5. By fitting the $\gamma\gamma$ mass and $E_\pi(1 - \cos\theta_\pi)$ distributions, the fraction of π^0 produced coherently is determined to be $19.5 \pm 1.1 \pm 2.5\%$. Excellent agreement is obtained between data and MC simulation.

2.3. Neutrino Oscillation Event Selection

MiniBooNE searches for $\nu_\mu \rightarrow \nu_e$ oscillations by measuring the rate of $\nu_e C \rightarrow e^- X$ CCQE events and testing whether the measured rate is consistent with the estimated background rate. To select candidate ν_e CCQE events, an initial selection is first applied: > 200 tank hits, < 6 veto hits, reconstructed time within the neutrino beam spill, reconstructed vertex radius < 500 cm, and visible energy $E_{vis} > 140$ MeV. It is then required that the event vertex reconstructed assuming an outgoing electron and the track endpoint reconstructed assuming an outgoing muon occur at radii < 500 cm and < 488 cm, respectively, to ensure good event reconstruction and efficiency for possible muon decay electrons. Particle identification (PID) cuts are then applied to reject muon and π^0 events. Several improvements have been made to the neutrino oscillation data analysis since the initial data was published²⁾, including an improved background estimate, an additional fiducial volume cut that greatly reduces the background from events produced outside the tank (dirt events),

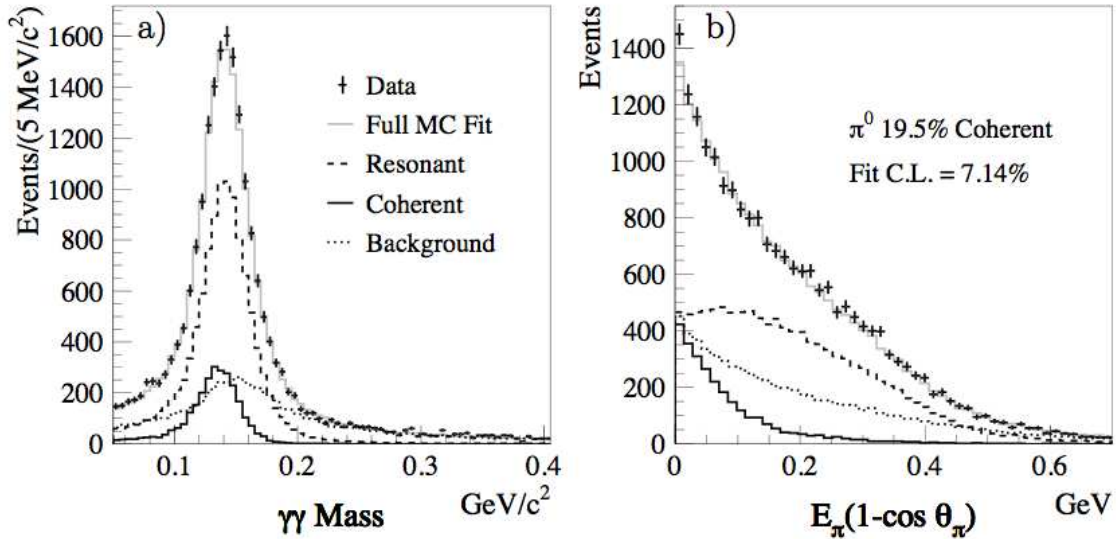


Figure 5: The neutral-current $\pi^0 \gamma\gamma$ mass and $E_\pi(1 - \cos\theta_\pi)$ distributions for data (points with error bars) compared to the MC simulation (histograms).

and an increase in the data sample from 5.579×10^{20} POT to 6.462×10^{20} POT. A total of 89,200 neutrino events pass the initial selection, while 1069 events pass the complete event selection of the final analysis with $E_\nu^{QE} > 200$ MeV, where E_ν^{QE} is the reconstructed neutrino energy.

2.4. Neutrino Oscillation Signal and Background Reactions

Table 1 shows the expected number of candidate ν_e CCQE background events with E_ν^{QE} between 200 – 300 MeV, 300 – 475 MeV, and 475 – 1250 MeV after the complete event selection of the final analysis. The background estimate includes antineutrino events, representing $< 2\%$ of the total. The total expected backgrounds for the three energy regions are 186.8 ± 26.0 events, 228.3 ± 24.5 events, and 385.9 ± 35.7 events, respectively. For $\nu_\mu \rightarrow \nu_e$ oscillations at the best-fit LSND solution of $\Delta m^2 = 1.2$ eV² and $\sin^2 2\theta = 0.003$, the expected number of ν_e CCQE signal events for the three energy regions are 7 events, 37 events, and 135 events, respectively.

2.5. Updated Neutrino Oscillation Results

Fig. 1 shows the reconstructed neutrino energy distribution for candidate ν_e data events (points with error bars) compared to the MC simulation (histogram)²⁾, while Fig. 6 shows the event excess as a function of reconstructed neutrino energy. Good agreement between the data and the MC simulation is obtained for $E_\nu^{QE} > 475$ MeV; however, an unexplained excess of electron-like events is observed for $E_\nu^{QE} < 475$

Table 1: *The expected number of events in the $200 < E_\nu^{QE} < 300$ MeV, $300 < E_\nu^{QE} < 475$ MeV, and $475 < E_\nu^{QE} < 1250$ MeV energy ranges from all of the significant backgrounds after the complete event selection of the final analysis. Also shown are the expected number of ν_e CCQE signal events for two-neutrino oscillations at the LSND best-fit solution.*

Process	200 – 300	300 – 475	475 – 1250
ν_μ CCQE	9.0	17.4	11.7
$\nu_\mu e \rightarrow \nu_\mu e$	6.1	4.3	6.4
NC π^0	103.5	77.8	71.2
NC $\Delta \rightarrow N\gamma$	19.5	47.5	19.4
Dirt Events	11.5	12.3	11.5
Other Events	18.4	7.3	16.8
ν_e from μ Decay	13.6	44.5	153.5
ν_e from K^+ Decay	3.6	13.8	81.9
ν_e from K_L^0 Decay	1.6	3.4	13.5
Total Background	186.8 ± 26.0	228.3 ± 24.5	385.9 ± 35.7
LSND Best-Fit Solution	7 ± 1	37 ± 4	135 ± 12

MeV. As shown in Fig. 6, the magnitude of the excess is very similar to what is expected from neutrino oscillations based on the LSND signal. Although the shape of the excess is not consistent with simple two-neutrino oscillations, more complicated oscillation models ^{4,5,6,7,8)} have shapes that may be consistent with both the LSND and MiniBooNE signals.

Table 2 shows the number of data, background, and excess events for different E_ν^{QE} ranges, together with the excess significance. For the final analysis, an excess of $128.8 \pm 20.4 \pm 38.3$ events is observed for $200 < E_\nu^{QE} < 475$ MeV. For the entire $200 < E_\nu^{QE} < 1250$ MeV energy region, the excess is $151.0 \pm 28.3 \pm 50.7$ events. As shown in Fig. 7, the event excess occurs for $E_{vis} < 400$ MeV, where E_{vis} is the visible energy.

Figs. 8 and 9 show the event excess as functions of Q^2 and $\cos(\theta)$ for events in the $300 < E_\nu^{QE} < 475$ MeV range, where Q^2 is determined from the energy and angle of the outgoing lepton and θ is the angle between the beam direction and the reconstructed event direction. Also shown in the figures are the expected shapes from $\nu_e C \rightarrow e^- X$ and $\bar{\nu}_e C \rightarrow e^+ X$ charged-current (CC) scattering and from the NC π^0 and $\Delta \rightarrow N\gamma$ reactions, which are representative of photon events produced by NC scattering. The NC scattering assumes the ν_μ energy spectrum, while the CC scattering assumes the transmutation of ν_μ into ν_e and $\bar{\nu}_e$, respectively. As shown in Table 3, the χ^2 values from comparisons of the event excess to the expected shapes are acceptable for all of the processes. However, any of the backgrounds in Table 3 would have to be increased by $> 5\sigma$ to explain the low-energy excess.

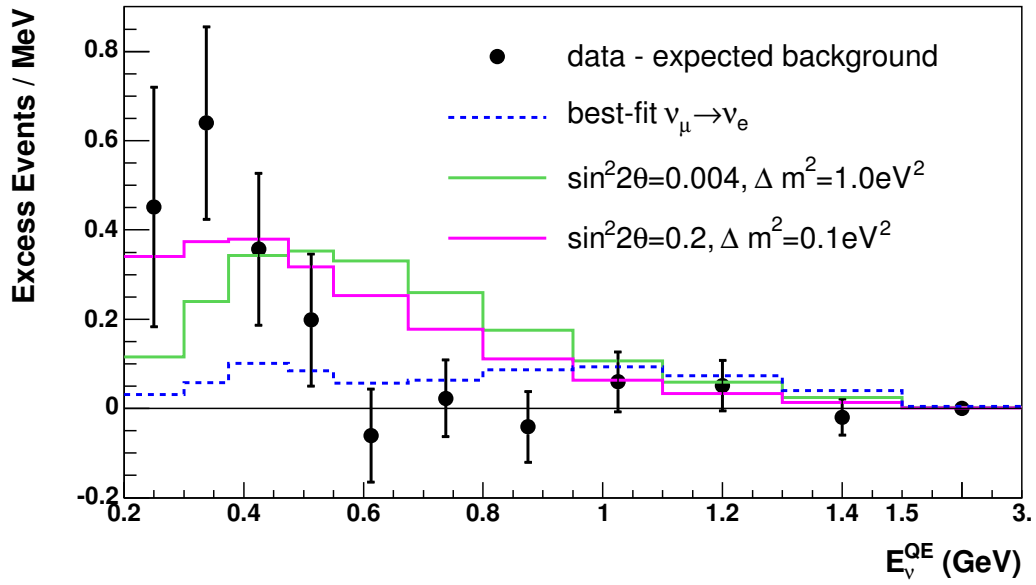


Figure 6: The event excess as a function of E_{ν}^{QE} . Also shown are the expectations from the best oscillation fit ($\sin^2 2\theta = 0.0017$, $\Delta m^2 = 3.14 \text{ eV}^2$) and from neutrino oscillation parameters in the LSND allowed region. The error bars include both statistical and systematic errors.

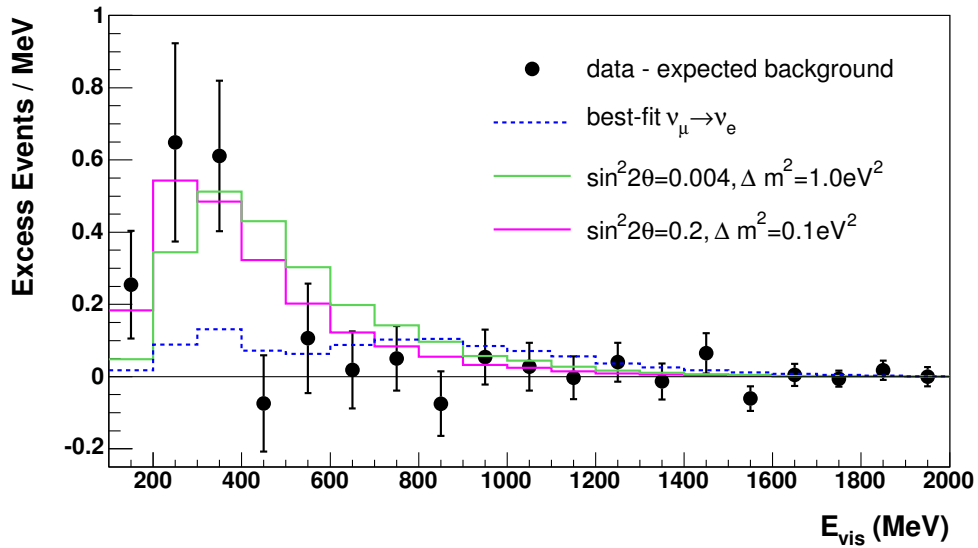


Figure 7: The event neutrino excess as a function of E_{vis} for $E_{\nu}^{QE} > 200 \text{ MeV}$. Also shown are the expectations from the best oscillation fit ($\sin^2 2\theta = 0.0017$, $\Delta m^2 = 3.14 \text{ eV}^2$) and from neutrino oscillation parameters in the LSND allowed region. The error bars include both statistical and systematic errors.

Table 2: The number of data, background, and excess events for different E_ν^{QE} ranges, together with the significance of the excesses in neutrino mode.

Event Sample	Final Analysis
200 – 300 MeV	
Data	232
Background	$186.8 \pm 13.7 \pm 22.1$
Excess	$45.2 \pm 13.7 \pm 22.1$
Significance	1.7σ
300 – 475 MeV	
Data	312
Background	$228.3 \pm 15.1 \pm 19.3$
Excess	$83.7 \pm 15.1 \pm 19.3$
Significance	3.4σ
200 – 475 MeV	
Data	544
Background	$415.2 \pm 20.4 \pm 38.3$
Excess	$128.8 \pm 20.4 \pm 38.3$
Significance	3.0σ
475 – 1250 MeV	
Data	408
Background	$385.9 \pm 19.6 \pm 29.8$
Excess	$22.1 \pm 19.6 \pm 29.8$
Significance	0.6σ

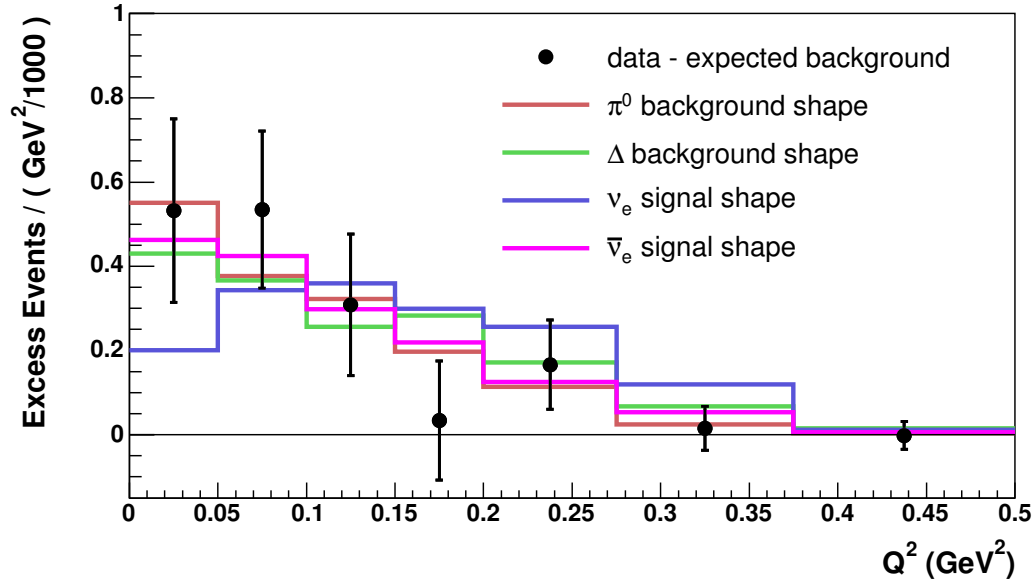


Figure 8: The neutrino event excess as a function of Q^2 for $300 < E_\nu^{QE} < 475$ MeV.

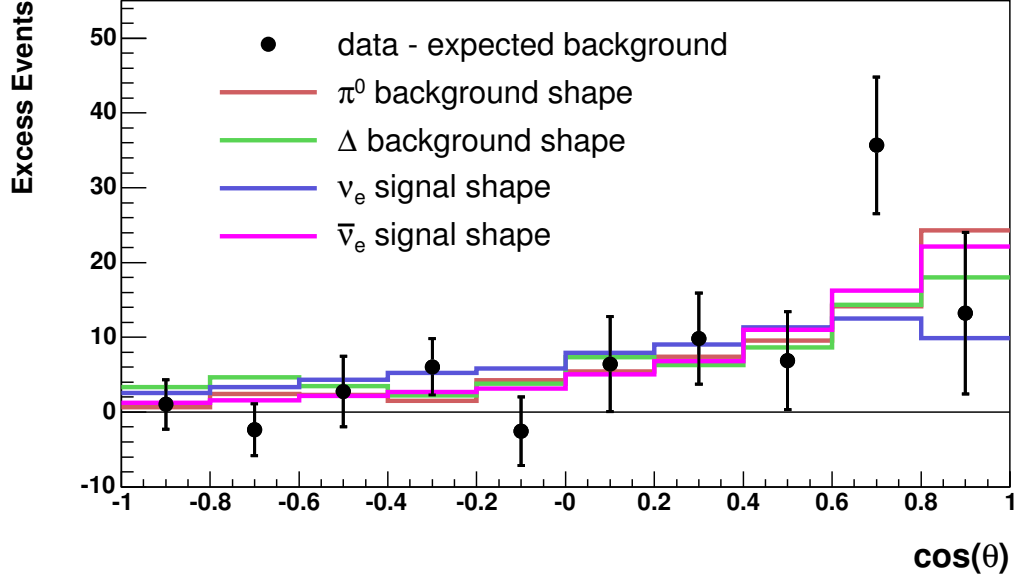


Figure 9: The neutrino event excess as a function of $\cos(\theta)$ for $300 < E_\nu^{QE} < 475$ MeV.

Table 3: The χ^2 values from comparisons of the neutrino event excess Q^2 and $\cos(\theta)$ distributions for $300 < E_\nu^{QE} < 475$ MeV to the expected shapes from various NC and CC reactions. Also shown is the factor increase necessary for the estimated background for each process to explain the low-energy excess.

Process	$\chi^2(\cos\theta)/9$ DF	$\chi^2(Q^2)/6$ DF	Factor Increase
NC π^0	13.46	2.18	2.0
$\Delta \rightarrow N\gamma$	16.85	4.46	2.7
$\nu_e C \rightarrow e^- X$	14.58	8.72	2.4
$\bar{\nu}_e C \rightarrow e^+ X$	10.11	2.44	65.4

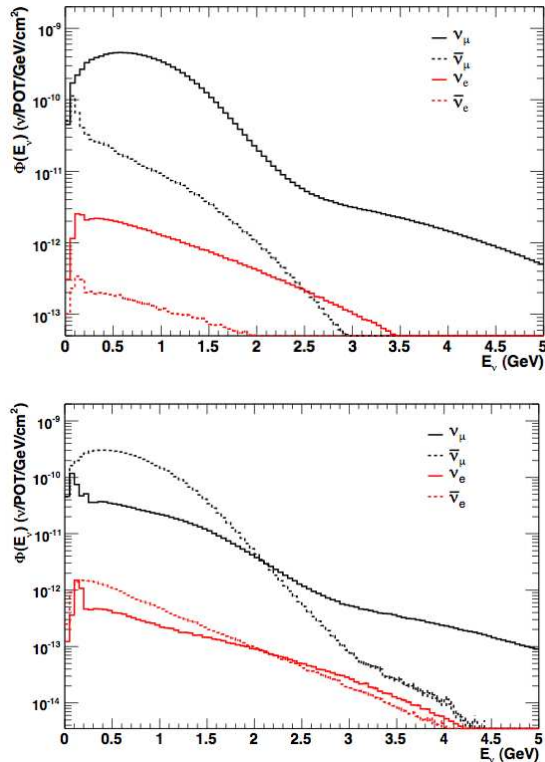


Figure 10: *The estimated neutrino fluxes for neutrino mode (top plot) and antineutrino mode (bottom plot).*

2.6. Initial Antineutrino Oscillation Results

The same analysis that was used for the neutrino oscillation results is employed for the initial antineutrino oscillation results²⁶⁾. Fig. 10 shows the estimated neutrino fluxes for neutrino mode and antineutrino mode, respectively. The fluxes are fairly similar (the intrinsic electron-neutrino background is approximately 0.5% for both modes of running), although the wrong-sign contribution to the flux in antineutrino mode ($\sim 18\%$) is much larger than in neutrino mode ($\sim 6\%$). The average ν_e plus $\bar{\nu}_e$ energies are 0.96 GeV in neutrino mode and 0.77 GeV in antineutrino mode, while the average ν_μ plus $\bar{\nu}_\mu$ energies are 0.79 GeV in neutrino mode and 0.66 GeV in antineutrino mode. Also, as shown in Fig. 11, the estimated backgrounds in the two modes are very similar, especially at low energy. Fig. 12 shows the expected antineutrino oscillation sensitivity for the present data sample corresponding to $3.4E20$ POT. The two sensitivity curves correspond to threshold neutrino energies of 200 MeV and 475 MeV.

The initial oscillation results for antineutrino mode are shown in Table 4 and Figs. 13 through 15. It is quite surprising that no excess ($-0.5 \pm 7.8 \pm 8.7$ events)

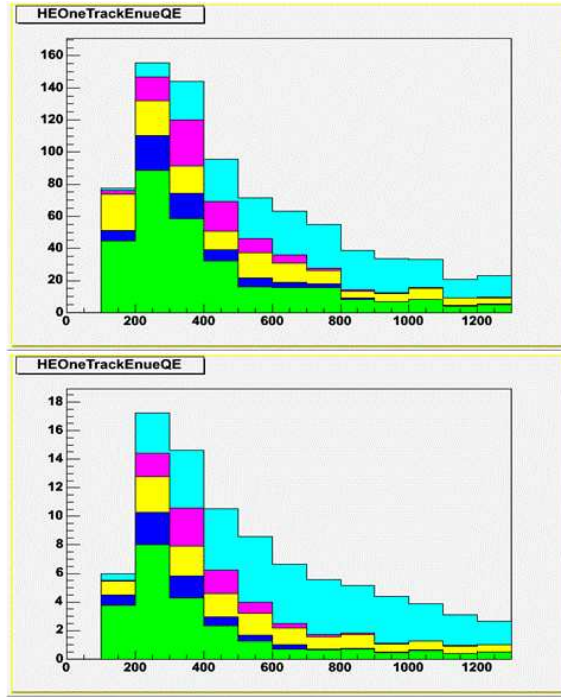


Figure 11: The estimated backgrounds for the neutrino oscillation search in neutrino mode (top plot) and antineutrino mode (bottom plot). The π^0 , $\Delta \rightarrow N\gamma$, intrinsic $\nu_e/\bar{\nu}_e$, external event, and other backgrounds correspond to the green, yellow, pink, light blue, blue, and cyan colors, respectively.

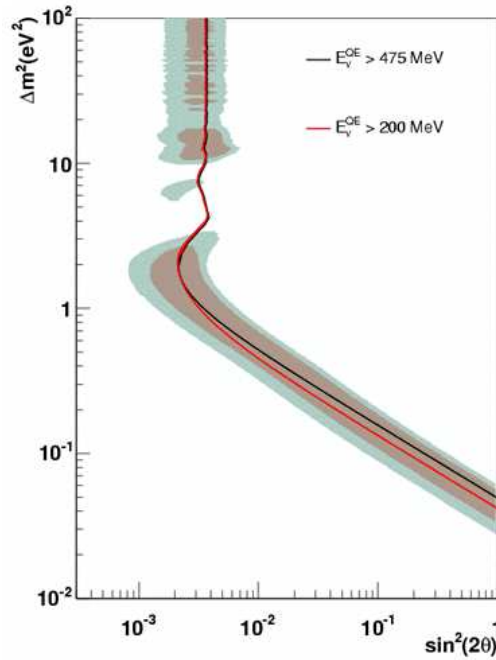


Figure 12: The expected antineutrino oscillation sensitivity at 90% CL for the present data sample corresponding to $3.4E20$ POT. The two sensitivity curves correspond to threshold energies of 200 MeV (red curve) and 475 MeV (black curve).

is observed in the low-energy range $200 < E_{\bar{\nu}}^{QE} < 475$ MeV. In order to understand the implications that the antineutrino data have on the neutrino low-energy excess, Table 5 shows the expected excess of low-energy events in antineutrino mode under various hypotheses. These hypotheses include the following:

- Same σ : Same cross section for neutrinos and antineutrinos.
- π^0 Scaled: Scaled to number of neutral-current π^0 events.
- POT Scaled: Scaled to number of POT.
- BKGD Scaled: Scaled to total background events.
- CC Scaled: Scaled to number of charged-current events.
- Kaon Scaled: Scaled to number of low-energy kaon events.
- Neutrino Scaled: Scaled to number of neutrino events.

Also shown in the Table is the probability (from a two-parameter fit to the data) that each hypothesis explains the observed number of low-energy neutrino and antineutrino events, assuming only statistical errors, correlated systematic errors, and uncorrelated systematic errors. A proper treatment of the systematic errors is in progress; however, it is clear from the Table that the “Neutrino Scaled” hypothesis fits best and that the “Same σ ”, “POT Scaled”, and “Kaon Scaled” hypotheses are strongly disfavored. It will be very important to understand this unexpected difference between neutrino and antineutrino properties.

The antineutrino data were also fit for oscillations in the energy range $475 < E_{\bar{\nu}}^{QE} < 3000$ MeV, assuming antineutrino oscillations but no neutrino oscillations. The antineutrino oscillation allowed region is shown in Fig. 16. At present, the oscillation limit is worse than the sensitivity. The best oscillation fit corresponds to $\Delta m^2 = 4.4$ eV², $\sin^2 2\theta = 0.0047$, and a fitted excess of 18.6 ± 13.2 events, which is consistent with the LSND best fit point of $\Delta m^2 = 1.2$ eV², $\sin^2 2\theta = 0.003$, and an expected excess of 14.7 events. With the present antineutrino statistics, the data are consistent with both the LSND best-fit point and the null point, although the LSND best-fit point has a better χ^2 ($\chi^2 = 17.63/15$ DF, probability = 30%) than the null point ($\chi^2 = 22.19/15$ DF, probability = 10%).

2.7. MiniBooNE NuMI Results

Neutrino events are also observed in MiniBooNE from the NuMI beam ²⁷⁾. The NuMI beam, as shown in Fig. 17, differs from the Booster neutrino beam (BNB) in several respects. First, the NuMI beam is off axis by 110 mrad, whereas the BNB is on axis. Second, neutrinos from NuMI travel ~ 700 m, compared to ~ 500 m for

Table 4: The number of antineutrino data, background, and excess events for different $E_{\bar{\nu}}^{QE}$ ranges, together with the significance of the excesses in antineutrino mode.

Event Sample	Final Analysis
200 – 475 MeV	
Data	61
Background	$61.5 \pm 7.8 \pm 8.7$
Excess	$-0.5 \pm 7.8 \pm 8.7$
Significance	-0.04σ
475 – 1250 MeV	
Data	61
Background	$57.8 \pm 7.6 \pm 6.5$
Excess	$3.2 \pm 7.6 \pm 6.5$
Significance	0.3σ
475 – 3000 MeV	
Data	83
Background	$77.4 \pm 8.8 \pm 9.6$
Excess	$5.6 \pm 8.8 \pm 9.6$
Significance	0.4σ

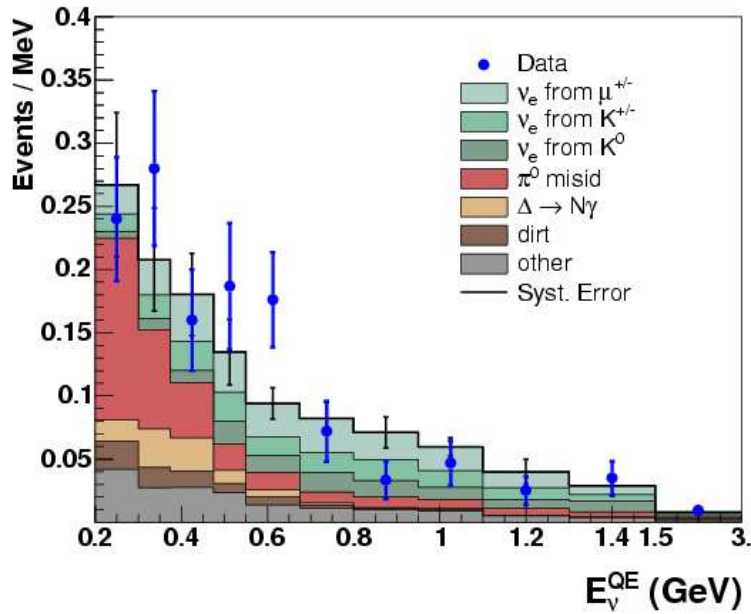


Figure 13: The comparison between data and Monte Carlo expectation as a function of reconstructed neutrino energy for the present antineutrino data sample corresponding to $3.4E20$ POT.

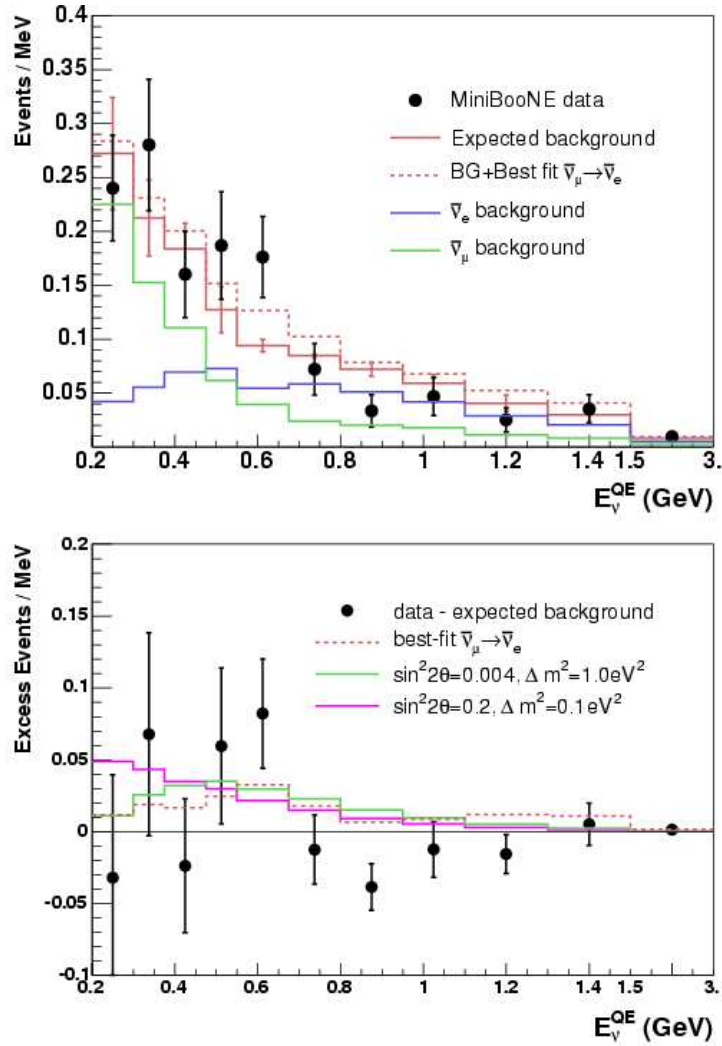


Figure 14: The comparison between data and Monte Carlo expectation (top) and the excess number of events (bottom) as a function of reconstructed neutrino energy for the present antineutrino data sample corresponding to $3.4E20$ POT. Also shown are the expectations from the best oscillation fit and from oscillation parameters in the LSND allowed region.

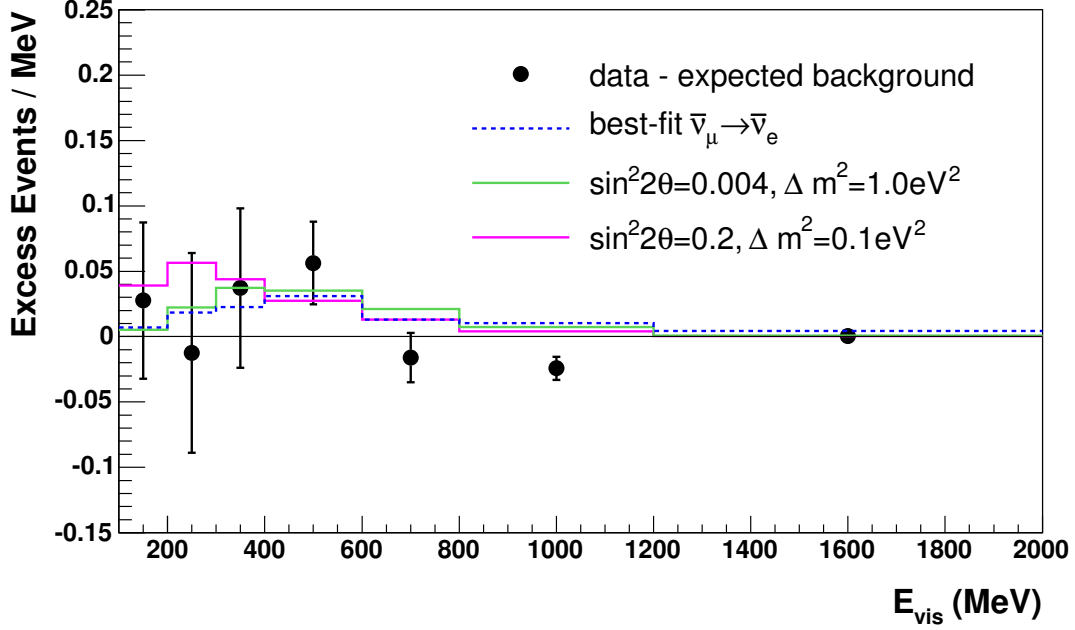


Figure 15: The excess number of events (data minus Monte Carlo expectation) as a function of visible energy for the present antineutrino data sample corresponding to $3.4E20$ POT. Also shown are the expectations from the best oscillation fit and from oscillation parameters in the LSND allowed region.

Table 5: The expected excess of low-energy events in antineutrino mode under various hypotheses for $3.4E20$ POT. Also shown in the Table is the probability (from a two-parameter fit to the data) that each hypothesis explains the observed number of low-energy neutrino and antineutrino events, assuming only statistical errors, correlated systematic errors, and uncorrelated systematic errors.

Hypothesis	# of $\bar{\nu}$ Events	Stat. Err.	Cor. Syst. Err.	Uncor. Syst. Err.
Same σ	37.2	0.1%	0.1%	6.7%
π^0 Scaled	19.4	3.6%	6.4%	21.5%
POT Scaled	67.5	0.0%	0.0%	1.8%
BKGD Scaled	20.9	2.7%	4.7%	19.2%
CC Scaled	20.4	2.9%	5.2%	19.9%
Kaon Scaled	39.7	0.1%	0.1%	5.9%
Neutrino Scaled	6.7	38.4%	51.4%	58.0%

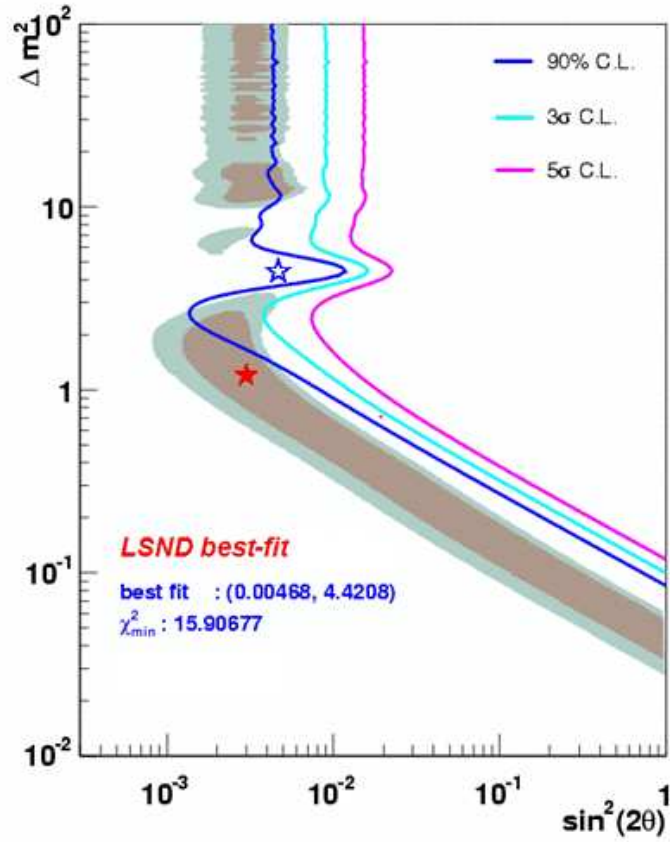


Figure 16: The antineutrino oscillation allowed region in the energy range $475 < E_{\bar{\nu}}^{QE} < 3000 \text{ MeV}$ for the present antineutrino data sample corresponding to $3.4E20 \text{ POT}$. Also shown are the best oscillation fit ($\Delta m^2 = 4.4 \text{ eV}^2$, $\sin^2 2\theta = 0.0047$, corresponding to an excess of 18.6 ± 13.2 events) and the LSND best fit point ($\Delta m^2 = 1.2 \text{ eV}^2$, $\sin^2 2\theta = 0.003$, corresponding to an excess of 14.7 events).

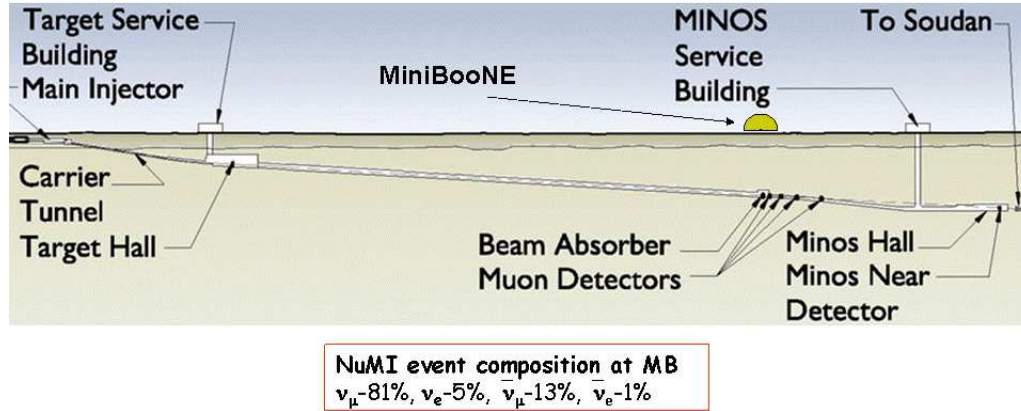


Figure 17: *The NuMI beam.*

neutrinos from the BNB. Also, the NuMI beam has a 6% contribution from electron-neutrinos and a 14% contribution from antineutrinos, while the BNB percentages are 0.5% and 2%, respectively. Fig. 18 shows the estimated neutrino flux at the MiniBooNE detector from the NuMI beam, while Fig. 19 compares the neutrino fluxes from the BNB and NuMI beams.

Figs. 20 and 21 show the comparison between data events (points with error bars) and the MC simulation (histogram) for ν_μ CCQE candidate events and ν_e CCQE candidate events, respectively. Although the systematic errors are presently large, the data are observed to be systematically low for ν_μ CCQE candidate events and systematically high for ν_e CCQE candidate events. Updated results should be available soon with three times the data sample and with reduced systematic errors by constraining the normalization to the ν_μ sample.

The NuMI data analysis is currently directed toward examining the low-energy region and searching for neutrino oscillations. This will complement the analysis done with MiniBooNE using neutrino and anti-neutrino BNB data, but with different systematic errors. It is worth noting that the NuMI ν_e CCQE sample has a very different composition when compared to the BNB neutrino ν_e CCQE sample. The BNB ν_e CCQE sample originates mostly from decays of pions and muons and contains a large fraction of ν_μ -induced mis-identified events. On other hand, the NuMI ν_e

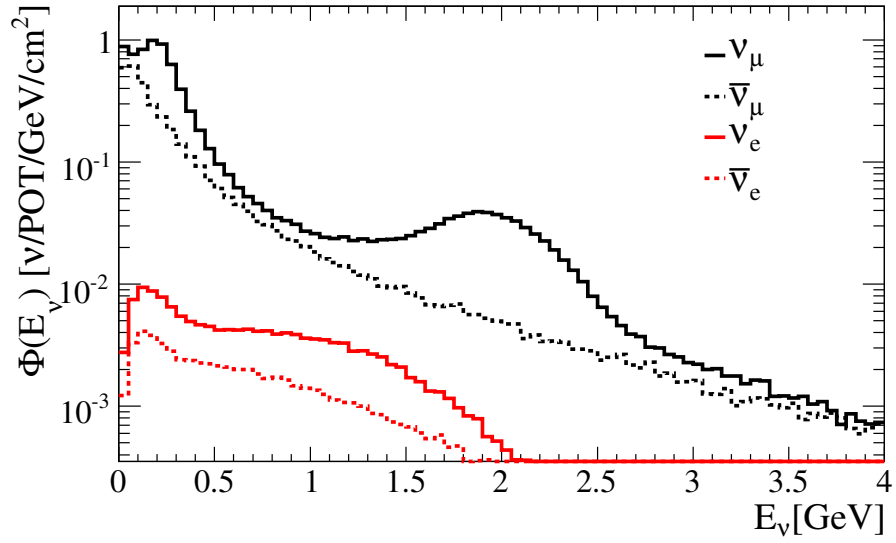


Figure 18: *The estimated neutrino flux at the MiniBooNE detector from the NuMI beam.*

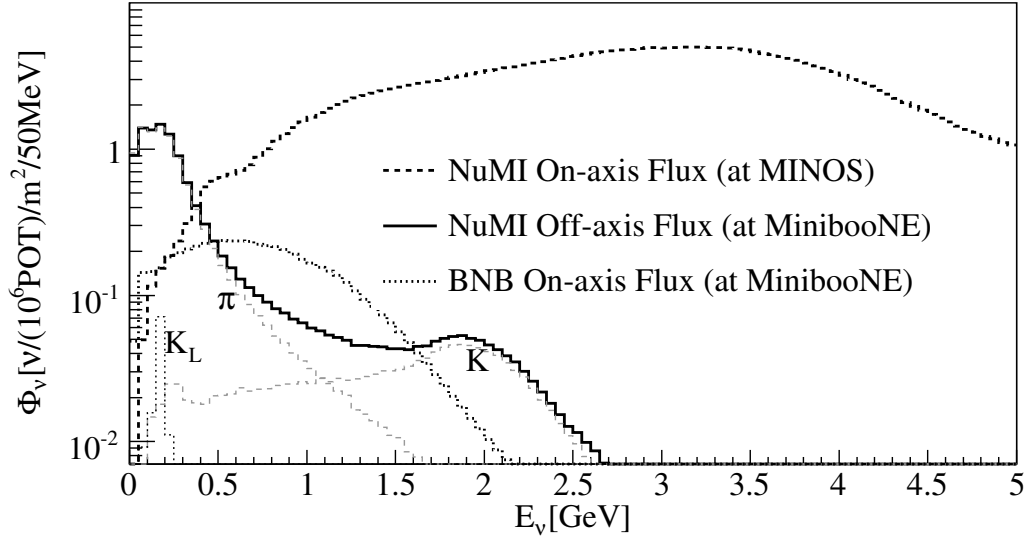


Figure 19: *A comparison between the BNB and NuMI neutrino fluxes.*

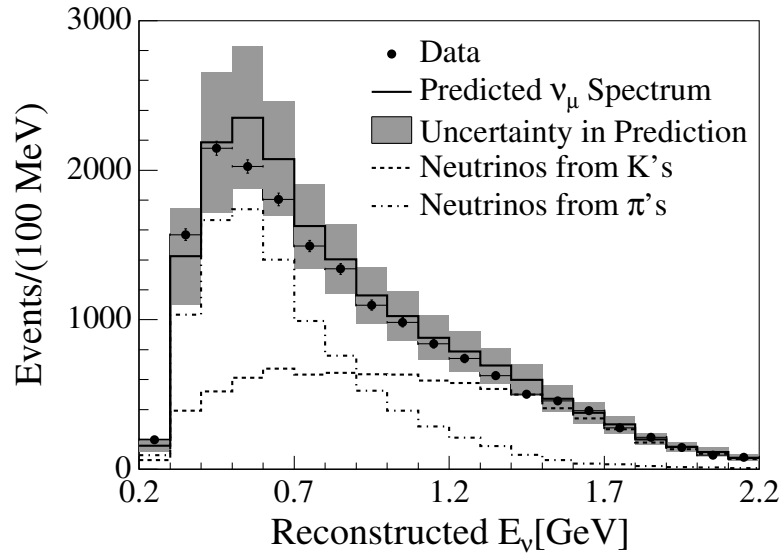


Figure 20: The comparison between data events (points with error bars) and the MC simulation (histogram) for NuMI-induced ν_μ CCQE candidate events.

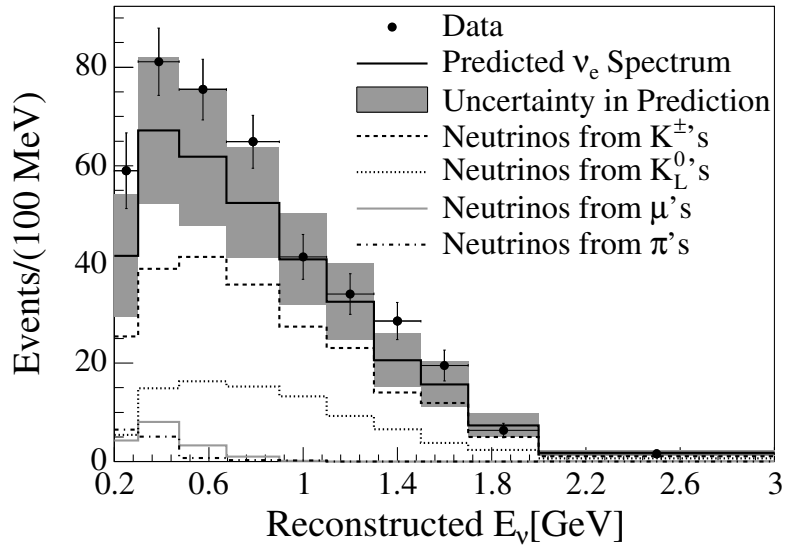


Figure 21: The comparison between data events (points with error bars) and the MC simulation (histogram) for NuMI-induced ν_e CCQE candidate events.

CCQE sample is produced mostly from the decay of kaons and contains a dominant fraction of intrinsic ν_e events. The analysis will be done by forming a correlation between the ν_μ CCQE and ν_e CCQE samples and by tuning the prediction to the data simultaneously. The result is that common systematics cancel, and this might reveal something important about the nature of the ν_e sample.

3. Physics Goals with 1E21 POT in Antineutrino Mode

MiniBooNE, so far, has collected $\sim 6.5 \times 10^{20}$ POT in neutrino mode and $\sim 3.4 \times 10^{20}$ POT in antineutrino mode. For the future, it is imperative to understand the MiniBooNE low-energy excess and to determine whether there is an unexpected difference between neutrino and antineutrino properties. The event excess in neutrino mode (and the apparent lack of an excess in antineutrino mode) is very interesting in its own right and important for future long-baseline experiments such as T2K, NO ν A, and LBNE. T2K will have a very similar neutrino energy distribution to MiniBooNE and will, therefore, be affected by the same low-energy excess. In addition, it is very important to test directly the LSND signal with a higher statistics antineutrino data sample.

3.1. Testing the Low-Energy Excess with Antineutrinos

With 1E21 POT in antineutrino mode, MiniBooNE will be able to determine conclusively whether there is an anomalous difference between neutrino and antineutrino properties. Table 6 shows the expected excess of low-energy events in antineutrino mode under various hypotheses for 1E21. Also shown in the Table is the probability (from a two-parameter fit to the data and assuming no excess in antineutrino mode) that each hypothesis explains the observed number of low-energy neutrino and antineutrino events, assuming only statistical errors, correlated systematic errors, and uncorrelated systematic errors. As can be seen in Table 6, the Neutrino Scaled hypothesis can be verified (and the other hypotheses rejected) with 1E21 POT if no excess is observed in antineutrino mode.

3.2. A Direct Test of the LSND signal with Antineutrinos

With 1E21 POT in antineutrino mode, MiniBooNE will be able to make a direct and fairly sensitive test of the LSND signal. For the best-fit LSND point of $\Delta m^2 = 1.2$ eV² and $\sin^2 2\theta = 0.003$ ¹⁾, MiniBooNE should observe in the $475 < E_\nu^{QE} < 3000$ MeV energy range an excess of $\sim 40.0 \pm 15.2 \pm 20.9$ events, corresponding to a $\sim 1.5\sigma$ signal. The significance of such a signal may be improved by further reductions in the systematic uncertainties (e.g. by comparing antineutrino data to neutrino data). Fig. 22 shows the expected antineutrino oscillation sensitivity for a threshold energy of

Table 6: *The expected excess of low-energy events in antineutrino mode under various hypotheses for 1E21 POT. Also shown in the Table is the probability (from a two-parameter fit to the data and assuming no excess in antineutrino mode) that each hypothesis explains the observed number of low-energy neutrino and antineutrino events, assuming only statistical errors, correlated systematic errors, and uncorrelated systematic errors.*

Hypothesis	# of $\bar{\nu}$ Events	Stat. Err.	Cor. Syst. Err.	Uncor. Syst. Err.
Same σ	111.6	0.0%	0.0%	4.7%
π^0 Scaled	58.2	0.1%	1.4%	17.1%
POT Scaled	202.5	0.0%	0.0%	1.3%
BKGD Scaled	62.7	0.1%	0.8%	15.0%
CC Scaled	61.2	0.1%	1.0%	15.6%
Kaon Scaled	119.1	0.0%	0.0%	4.0%
Neutrino Scaled	20.1	17.2%	44.1%	54.5%

475 MeV. The curves correspond to 3.4E20 POT, 5E20 POT, and 1E21 POT. With 1E21 POT, most of the LSND region is covered at 90% CL.

3.3. MiniBooNE Follow-On

For the future, it will be imperative to understand the MiniBooNE low-energy excess. This excess is very interesting in its own right and important for future long-baseline experiments such as T2K, NO ν A, and LBNE. T2K will have a very similar neutrino energy distribution to MiniBooNE and will, therefore, be affected by the same low-energy excess. By analyzing the MiniBooNE antineutrino data, NuMI data, and SciBooNE data, it may be possible to reduce systematic errors and determine whether any of the published models ^{3,4,5,6,7,8)} can provide an explanation for the excess. A full error matrix with correlated and uncorrelated systematic errors is used to estimate the systematic error at low energies and includes errors from neutrino flux, neutrino cross sections, and detector response. By comparing data sets, some of these systematic errors will cancel. If the low-energy excess continues to be consistent with a signal, then new experiments at FNAL (MicroBooNE and BooNE) or ORNL (OscSNS) should be built to explore physics beyond the Standard Model.

4. MicroBooNE

The MicroBooNE experiment ²⁸⁾, which was recently approved at Fermilab, exploits the precise differentiation of photons versus electrons in a detector, as is uniquely available from a Liquid Argon Time Projection Chamber (LArTPC). The detector consists of a ~ 70 ton fiducial volume LArTPC. It will run near the MiniBooNE enclosure on the BNB with an expected exposure of 6×10^{20} protons on target. Approximately 10^5 events will be collected with the BNB and about 6×10^4 events

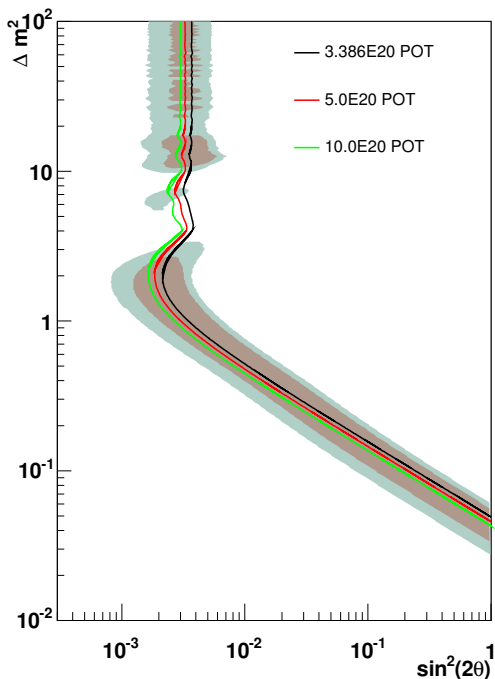


Figure 22: The expected antineutrino oscillation sensitivity for a threshold energy of 475 MeV. The curves correspond to 3.4E20 POT, 5E20 POT, and 1E21 POT.

with the off-axis NuMI beam. The high spatial resolution and energy measurement down to the MeV scale will substantially improve on information available from the MiniBooNE detector. The experiment will run in 2011.

The MicroBooNE detector, as shown in Fig. 23, can separate electron showers from photon showers using the energy deposited in the first 2.4 cm of the track. For an electron efficiency of 80%, γ contamination is expected to be $< 5\%$, based on MC studies. The electron and γ energy resolution is $< 10\%$ for energies above 15 MeV. Given the excellent e/γ separation, MicroBooNE can identify the source of the low energy events observed in MiniBooNE. MicroBooNE's sensitivity to the low energy excess is $\sim 5\sigma$ if the signal is electron-like and $\sim 3\sigma$ if the signal is photon-like, in a strictly counting-based experiment. Fits to shape-signatures may increase the significance.

5. BooNE

The BooNE experiment would involve building a second detector at a cost of $\sim \$8\text{M}$ along the BNB at FNAL at a different distance. With two detectors, many of the systematic errors would cancel, as the neutrino flux varies as $1/r^2$ to good approximation, so that a simple ratio of events in the two detectors would provide a sensitive search for ν_e appearance and ν_μ disappearance. Furthermore, by comparing the rates for a NC reaction, such as NC π^0 scattering or NC elastic scattering, a

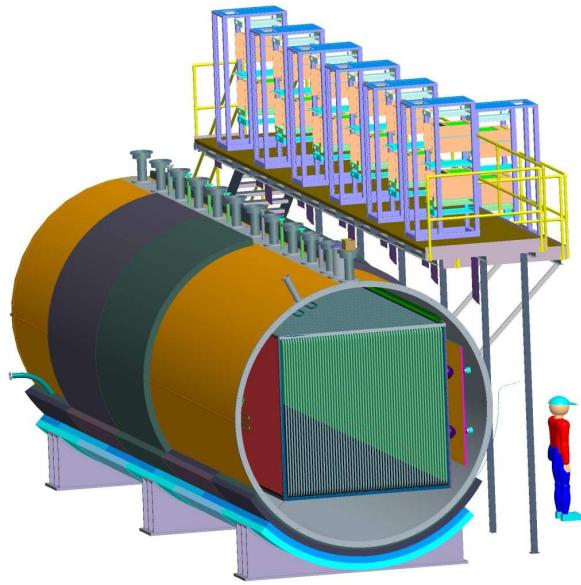


Figure 23: A schematic drawing of the MicroBooNE detector.

sensitive search for sterile neutrinos can be made.

An even cheaper option would be to move the MiniBooNE detector to a different location at a cost of only $\sim \$3\text{M}$. For example, if the MiniBooNE detector were moved to a distance of 200 m from the neutrino source, then the event rate would increase by a factor of ~ 6 due to the $1/r^2$ dependence of the neutrino flux. After a year of running, the comparison of the event rates at the two locations could determine whether the low-energy excess observed by MiniBooNE was due to neutrino oscillations. In addition, ν_μ and $\bar{\nu}_\mu$ disappearance could be searched for with high precision in the $\Delta m^2 > 0.1 \text{ eV}^2$ mass region.

6. OscSNS

The OscSNS experiment ²⁹⁾ would involve building a MiniBooNE-like detector at a distance of ~ 60 m from the SNS beam dump at ORNL. The detector would be the same as MiniBooNE except with a higher phototube coverage of 25% and the addition of $\sim 0.031 \text{ g/l}$ of butyl-PBD scintillator. Due to the higher phototube coverage, the estimated cost is $\sim \$12\text{M}$. Fig. 24 shows the layout of the SNS, which is running with a proton energy of 1 GeV with a goal of eventually reaching a beam power of ~ 1.4 MW. The great advantage of the SNS is that the neutrino flux is extremely intense and known almost perfectly, and the neutrino cross sections are known well. Fig. 25 shows the neutrino flux energy distribution, which includes a monoenergetic 30 MeV

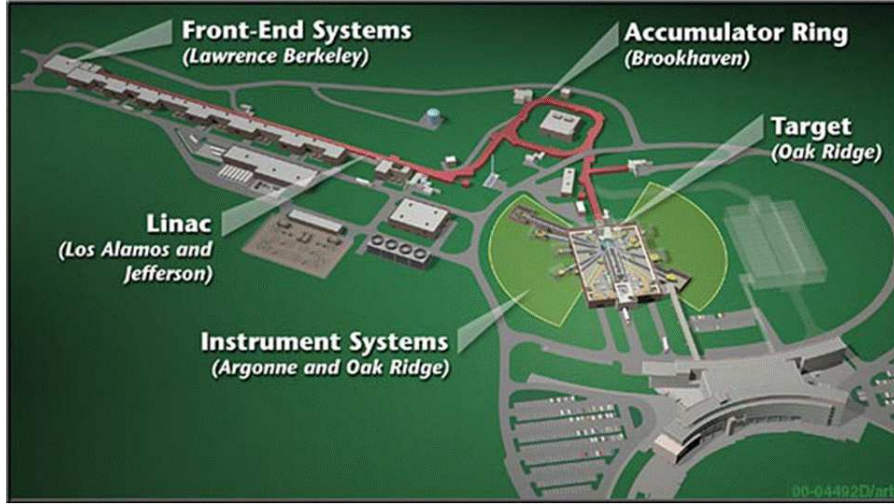


Figure 24: *The layout of the SNS.*

ν_μ from π^+ DAR and ν_e and $\bar{\nu}_\mu$ from μ^+ DAR. Furthermore, as shown in the left plot of Fig. 25, the monoenergetic ν_μ can be identified by timing, as was performed by the KARMEN experiment at the ISIS proton accelerator.

With the SNS neutrino flux, OscSNS would be capable of making precision measurements of ν_e and $\bar{\nu}_e$ appearance and ν_μ disappearance and proving the existence of sterile neutrinos via the NC reaction $\nu_\mu C \rightarrow \nu_\mu C^*$ (15.11). Any observed reduction of this cross section would be evidence for active-sterile neutrino oscillations. Fig. 26 shows the expected active-sterile neutrino oscillation sensitivity as a function of Δm^2 and $\sin^2 2\theta$ ²⁹⁾. Fig. 27 shows the expected $\bar{\nu}_e$ appearance sensitivity. Other physics goals include precision measurements of $\nu e \rightarrow \nu e$ elastic scattering (and the world's best sensitivity for the ν_μ magnetic moment) and $\nu_e C \rightarrow e^- N$ charged-current scattering.

7. Conclusion

The MiniBooNE experiment observes an unexplained excess of electron-like events at low energies in neutrino mode, which may be due, for example, to either a neutral current radiative interaction ³⁾ or to neutrino oscillations involving sterile neutrinos ^{4,5,6,7,8)} and which may be related to the LSND signal. No excess of electron-like events, however, is observed so far at low energies in antineutrino mode. MiniBooNE, therefore, has requested additional running in antineutrino mode for a total of 1E21

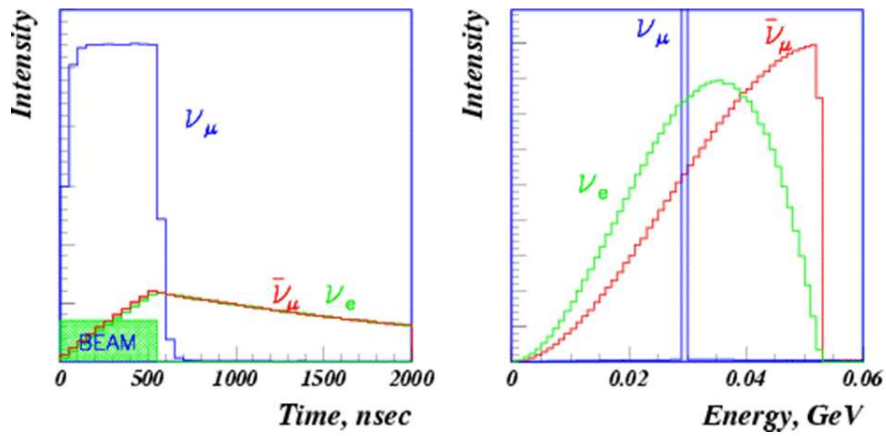


Figure 25: The right plot shows the neutrino flux energy distribution, which includes a monoenergetic 30 MeV ν_μ from π^+ DAR and ν_e and $\bar{\nu}_\mu$ from μ^+ DAR. The left plot shows the neutrino time distribution. The monoenergetic ν_μ can be identified by timing.

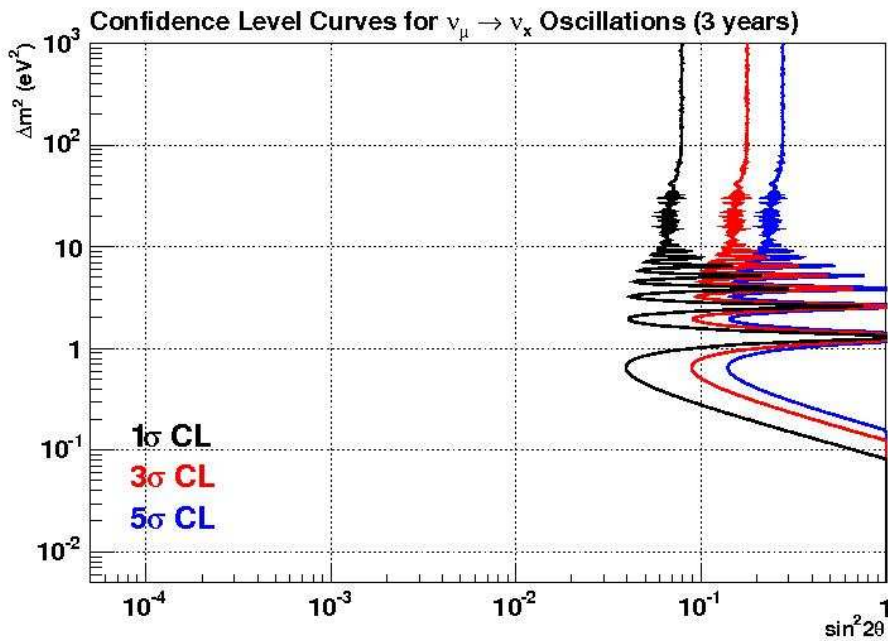


Figure 26: The expected OscSNS active-sterile neutrino oscillation sensitivity as a function of Δm^2 and $\sin^2 2\theta$ after three years of data taking.

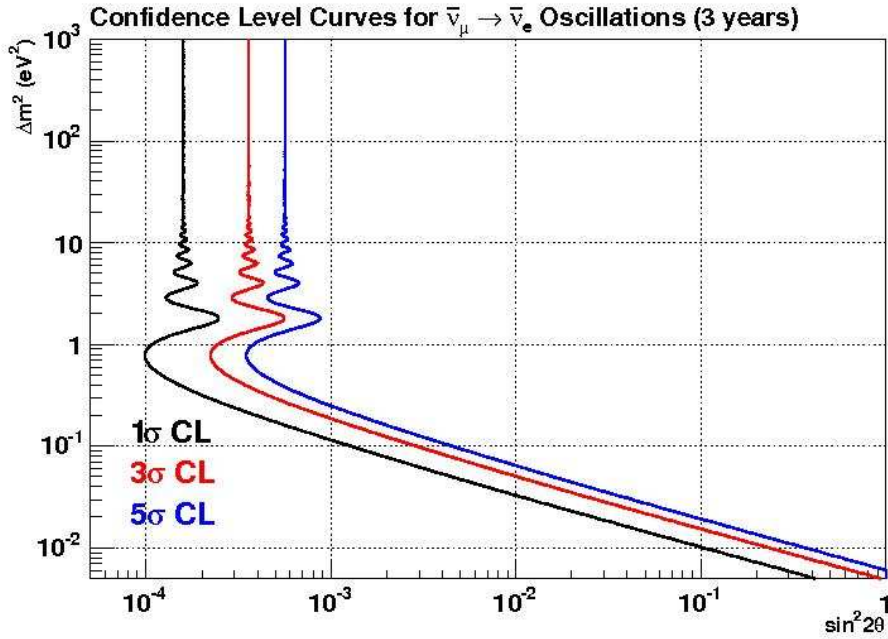


Figure 27: The expected OscSNS $\bar{\nu}_\mu \rightarrow \bar{\nu}_e$ oscillation sensitivity as a function of Δm^2 and $\sin^2 2\theta$ after three years of data taking.

POT. With this additional data taking, which should be completed by the end of 2011, the MiniBooNE collaboration will be able to determine conclusively whether there is an anomalous difference between neutrino and antineutrino properties.

In addition, the high energy antineutrino data will provide a direct test of the LSND signal and will increase the statistics of the NuMI data sample. With the present $3.4E20$ POT in antineutrino mode, almost all of the LSND region is still allowed, as the current limit is worse than the sensitivity. However, with $1E21$ POT in the case of no neutrino oscillations, most of the LSND allowed region should be ruled out. In the case of neutrino oscillations at the LSND best-fit point, a $\sim 1.5\sigma$ event excess would be expected.

If the low-energy excess continues to be consistent with a signal, then new experiments at FNAL (MicroBooNE and BooNE) or ORNL (OscSNS) should be built to explore physics beyond the Standard Model.

8. Acknowledgements

We thank Milla Baldo Ceolin for the invitation to make a presentation at this stimulating conference and for her superb organization of the conference.

9. References

- 1) C. Athanassopoulos *et al.*, Phys. Rev. Lett. 75, 2650 (1995); 77, 3082 (1996); 81, 1774 (1998); A. Aguilar *et al.*, Phys. Rev. D 64, 112007 (2001).
- 2) A. Aguilar-Arevalo *et al.*, Phys. Rev. Lett. 98, 231801 (2007); A. Aguilar-Arevalo *et al.*, Phys. Rev. Lett. 102, 101802 (2009).
- 3) Jeffrey A. Harvey, Christopher T. Hill, Richard J. Hill, [arXiv:0708.1281]; [arXiv:0712.1230].
- 4) Michel Sorel, Janet Conrad, and Michael Shaevitz, Phys. Rev. D 70, 073004 (2004); C. Karagiorgi *et al.*, Phys. Rev. D 75, 013011 (2007); Alessandro Melchiorri *et al.*, [arXiv:0810.5133].
- 5) Heinrich Paes, Sandip Pakvasa, Thomas J. Weiler, Phys. Rev. D 72, 095017 (2005); [arXiv:hep-ph/0504096].
- 6) T. Goldman, G. J. Stephenson Jr., and B. H. J. McKellar, Phys. Rev. D 75, 091301 (2007).
- 7) Michele Maltoni and Thomas Schwetz, Phys. Rev. D 76, 093005 (2007); [arXiv:0705.0197].
- 8) Ann E. Nelson and Jonathan Walsh, [arXiv:0711.1363].
- 9) B. T. Cleveland *et al.*, Astrophys. J. 496, 505 (1998).
- 10) J. N. Abdurashitov *et al.*, Phys. Rev. C 60, 055801 (1999).
- 11) W. Hampel *et al.*, Phys. Lett. B 447, 127 (1999).
- 12) S. Fukuda *et al.*, Phys. Lett. B 539, 179 (2002).
- 13) Q. R. Ahmad *et al.*, Phys. Rev. Lett. 87, 071301 (2001); Q. R. Ahmad *et al.*, Phys. Rev. Lett. 89, 011301 (2002); S. N. Ahmed *et al.*, Phys. Rev. Lett. 92, 181301 (2004).
- 14) K. Eguchi *et al.*, Phys. Rev. Lett. 90, 021802 (2003); T. Araki *et al.*, Phys. Rev. Lett. 94, 081801 (2005).
- 15) K. S. Hirata *et al.*, Phys. Lett. B 280, 146 (1992); Y. Fukuda *et al.*, Phys. Lett. B 335, 237 (1994).
- 16) Y. Fukuda *et al.*, Phys. Rev. Lett. 81, 1562 (1998).
- 17) W. W. M. Allison *et al.*, Phys. Lett. B 449, 137 (1999).
- 18) M. Ambrosio *et al.*, Phys. Lett. B 517, 59 (2001).
- 19) M. H. Ahn *et al.*, Phys. Rev. Lett. 90, 041801 (2003).
- 20) D. G. Michael *et al.*, Phys. Rev. Lett. 97, 191801 (2006); P. Adamson *et al.*, Phys. Rev. Lett. 101, 131802 (2008).
- 21) T. Katori, A. Kostelecky and R. Tayloe, Phys. Rev. D 74, 105009 (2006).
- 22) A. Aguilar-Arevalo *et al.*, [arXiv:0806.1449].
- 23) A. Aguilar-Arevalo *et al.*, Nucl. Instr. Meth. **A559**, 28 (2009).
- 24) A. Aguilar-Arevalo *et al.*, Phys. Rev. Lett. 100, 032301 (2008).
- 25) A. Aguilar-Arevalo *et al.*, Phys. Lett. 664B, 41 (2008).
- 26) A. Aguilar-Arevalo *et al.*, [arXiv:0904.1958].
- 27) P. Adamson *et al.*, [arXiv:0809.2447].
- 28) H. Chen *et al.*, A Proposal for a New Experiment Using the Booster and NuMI Neutrino Beamlines: MicroBooNE (2007).
- 29) G. T. Garvey *et al.*, Phys. Rev. D 72, 092001 (2005).